HUNGARIAN UNIVERSITY OF
AGRICULTURE AND LIFE SCIENCES

Solar heat for food industry processes

PhD Dissertation

by

Rajab Ghabour

Gödöllő
2024

Doctoral school

Denomination: Doctoral School of Mechanical Engineering

Science: Mechanical Engineering

Leader: Prof. Dr. Gábor Kalácska, DSc
Institute of Technology
Hungarian University of Agriculture and Life Sciences,
Szent István Campus, Gödöllő, Hungary

Supervisor: Dr. habil. Péter Korzenszky, PhD
Institute of Technology
Hungarian University of Agriculture and Life Sciences,
Szent István Campus, Gödöllő, Hungary

……...…… ….....……

Affirmation of supervisor Affirmation of head of school

CONTENTS

1. INTRODUCTION, OBJECTIVES 4
2. MATERIALS AND METHODS 6
2.1. PCM integration into TES 6
2.2. Model development and simulation of tankless SHIP 7
2.2.1. SHIP concept 7
*2.2.2. Modelling in T*sol 7*
2.2.3. Experiment configurations 8
2.3. Boiler configurations within the SHIP system 10
3. RESULTS AND DISCUSSION 13
3.1. Experimental results of integrating PCM Soy wax into TES 13
3.1.1. Statistical analysis of the soy waxes results 14
3.2. Optimum boiler configurations into SHIP 16
3.2.1. Required collector area 16
3.2.2. Glycol ratio configurations 17
3.2.3. Collector flow rate configuration 17
3.2.4. Relative tank volume configuration 17
3.2.5. Tank height-to-diameter configuration 18
3.2.6. Overall system response to changing factors using RSM method 18
3.3. Tankless SHIP 20
3.3.1. Hungarian weather profile 20
3.3.2. Model validation 21
3.3.3. Parametric analysis 23
4. NEW SCIENTIFIC RESULTS 26
5. CONCLUSION AND SUGGESTIONS 30
6. SUMMARY 32
7. ÖSSZEFOGLALÁS (SUMMARY IN HUNGARIAN) 34

1. INTRODUCTION, OBJECTIVES

A substantial amount of heat energy demand can be obtained from solar thermal systems for industrial and agri-food processes, where 77% of the energy needed in Agri-processing is for heating processes (60% of the heat needed must be below 250 ℃). Up to 400 ℃ steam or hot water can be supplied in developed economies, giving a chance to cover about half of the energy demand. Also, the variation in industry sectors from food, textile, brick, and agriculture processes match the variation in the solar thermal energy types like hot water or hot air, which are suitable for drying, washing, dyeing, boiling, pasteurization and sterilization.

The agri-Food sector is also famous for many problems: high carbon emissions, packaging waste, and food waste with massive consumption of water and land, so sustainability is needed urgently in this sector. Any slight improvement in machines, storage, and energy consumption can lead to massive savings.

This research will lead to a better understanding and optimising of the solar heat for industrial process systems and provide an overall view of the influencing factors from the first and second degrees and the two factors' interactions. This novel cross-over research area will allow the collection of a unique and new prospective dataset. Based on the results, recommendations will be formulated for industrial applications from micro and macro levels. These new findings will be helpful for industrial plants and decision-makers willing to integrate and utilise solar thermal energy not just for final heat processing usage but also for preheating purposes. MeteoSyn and T*Sol software will extract the meteorological data and operate the simulation process. For the programming process, R-script software is used to identify the essential factors illustrated by Pareto Plots and the two-factor interactions and done by non or linear modelling using the response surface method (RSM). Then, those data are validated and compared with the real-time measurements. Finally, the optimums parameters are identified using Lagrange optimum conditions. The experiments and measurements will consider the most influential factors: collector area, volume flow rate, glycol ratio, tank height to diameter ratio, relative tank capacity, PCM quantity, PCM specimens, and temperature. The general objective of this study is to investigate the technical challenges of integrating food industries with a solar heat system, considering the general assessment of different solar collector types and thermal energy storage enhancement using phase change materials for some parts.

The detailed research objectives can be described as the following:

a) What is the influence of integrating PCM materials such as Soy wax (52℃ and 62℃ melting temperature) as encapsulated specimens into the solar thermal tank for low-temperature thermal processes?
b) Comparison of the performance of the two Soy waxes and determining the optimum operating values using Lagrange optimum conditions.
c) Comparison of the in-series and in-parallel boiler configuration performance in the solar heat for industrial process.
d) Evaluation of the performance of the tankless solar thermal system under Hungarian weather conditions as a preheating system for industrial processes using low temperatures.
e) What are the optimum flow rates for the primary and secondary circuits for generating the highest energy (kWh) or temperature (℃) of the secondary circuit?

2. MATERIALS AND METHODS

This chapter presents the materials, equipment, procedures, and processes employed in the current research. It also includes the experimental measurements' scientific methods and the test systems' description to accomplish the set research aims.

2.1. PCM integration into TES

The laboratory conducted mathematical and experimental modelling of a Soy wax PCM integrated into the solar tank using the response surface method. A capsulated PCM Soy wax 52℃ and 62℃ in a 5 litre insulated water tank was conducted. The response surface approach with non-linear correlation was used for the charging phase to determine the appropriate number of samples and the quantity of PCM at two temperature levels. The method will illustrate the first-degree effect of the Temperature, sample numbers, and wax quantity. Furthermore, each two-factor interaction contour plot is depicted.

The experiment components are a water tank, heater, sensors, datalogger (ALMEMO 2890-9), and wax. The system comprises a well-insulated water tank with 5 cm of EPS. The experiment continues until the internal temperature of the tank approaches the ambient temperature by a difference of 1℃. Equation 2.1 shows how the heat balance difference is calculated:

$$T_{avg\_tank} - T_{amb} \leq +1\ ℃ \tag{2.1}$$

The experiment aims to determine the system's thermal inertia time (τ (h)), i.e. the time it takes for the tank to cool down to ambient temperature.

The model was built using the R programming language, with coded values ranging from [-1, +1] for each variable, and the variables being "S" for Sample numbers. The quantity of PCM in each sample is denoted by the letter "Q". Finally, the temperature is represented by the letter "T". The number of experiments is determined using the form 2^k, where k is the number of variables, therefore $2^{3,}$ resulting in eight measurements, as in Table 2.1. To detect the second-degree non-linear coefficients, additional measurement was undertaken inside or outside the border of the cube to illustrate the non-linear effects.

Equation 2.2 represents the relationship transferring between coded values and real values:

$$Coded\ value = \frac{Real\ value - Center\ point}{\frac{1}{2}(range)} \tag{2.2}$$

Table 2.1. Number of settings and model values of experimental parameters

Number of experimental setups	1	2	3	4	5	6	7	8
S - Samples	-1	+1	-1	+1	-1	+1	-1	+1
Q - Quantity (g)	-1	-1	+1	+1	-1	-1	+1	+1
T - Temperature (℃)	-1	-1	-1	-1	+1	+1	+1	+1

2.2. Model development and simulation of tankless SHIP

A dynamic analysis tool is needed to accurately describe the system's response to the rapid environmental change in weather conditions to study the SHIP system's performance. The calculations are based on the energy balance flows and provide predictions according to the hourly meteorological data.

2.2.1. SHIP concept

The SHIP comprises a solar collector integrated with an external heat exchanger in a closed loop. The concept assumes that the flow goes out of the solar collector at a specific temperature (denoted by $T_{Pr\ In}$). Moreover, the output temperature from the heat exchanger in the primary loop (denoted by $T_{Pr\ Out}$) is the same temperature that flows in the collector. On the secondary side of the heat exchanger, there is an open loop that warms up the network water (denoted by $T_{Sec\ In}$) by exchanging the heat with the fluid on the primary side so it can be ready for the heat process at the required temperature (denoted by $T_{Sec\ Out}$). The schematic concept of the system is shown in Fig. 2.1.

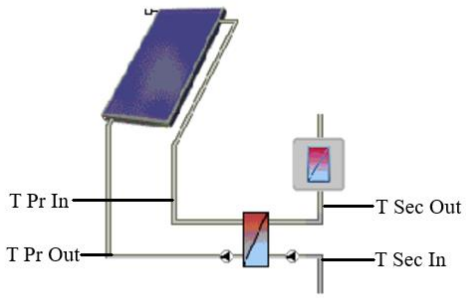

Fig. 2.1. A tankless solar system with heat exchanger and FPC collector schematic where: T- temperature, Pr- primary side, Sec- secondary side, In- input and Out- output

*2.2.2. Modelling in T*sol*

The simulation is carried out using the outputs of the six actual experiments to reach the optimum operating configuration from two aspects: the highest output temperature and the highest energy gain. These different configurations of the

food process industry aim to assess and optimize the working parameters according to the Hungarian meteorological conditions.

2.2.3. Experiment configurations

The components used in the T*sol model configuration are (1) single FPC. (2) external heat exchanger transfers the absorbed energy from the primary loop to the secondary one. (3) heat exchanger as described in Fig.2.2. The water flows in the pipes using an active circulation pump in a closed loop in the primary loop. The flow rate of the primary loop is 60 litres per hour. The fluid is a mixture of glycol and water with an 18% volumetric percentage to avoid freezing and bursting during low temperatures.

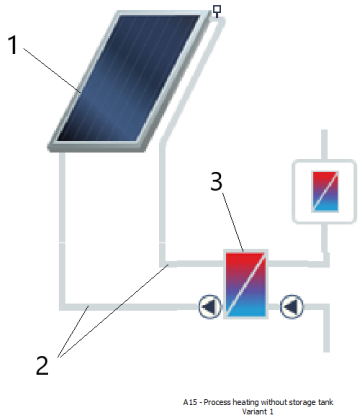

Fig 2.2 T*sol model configuration where: 1) Solar collector, 2) piping system, 3) heat exchanger.

The intended experimental setup consists of several primary data logging and instrumentation components as in Fig. 2.3: (1) IMRe, (2) data logger (ALMEMO® 2890-9) in a universal input data logger that connects nine sensors through multiple channels, (3) pyranometer, (4) mechanical flow meter, (5) temperature sensor (K-type). (6) Open Energy Monitor is a monitoring, modelling, and assessment tool to monitor live data and records. (7) TECH controller to adjust the working schedule of the process heat.

Fig. 2 IMRe controlling system

1) IMRe 2) Data logger 3) Pyranometer 4) flow meter 5) Temperature sensor 6) Energy monitoring software

The experiment set up has been installed in the Hungarian University of Agriculture and Life Sciences renewable energy laboratory, Gödöllő, Hungary. Experiments were carried out 24 hours a day during August and September 2021, when the weather was relatively stable, with rain interruptions for a few days during the whole period. All the data have been recorded persistently by the data logger every minute.

The actual experiment (mainly the solar collector) was mounted on a metallic structure and directed at an angle of 33º facing the south to harvest the maximum solar radiations throughout the day.

2.3. Boiler configurations within the SHIP system

An indirectly forced circulations solar thermal system for heat process applications with external heat exchanger integration and antifreeze fluid in the primary flow loop is modelled in this study. The secondary loop is the process heat section where the boiler is connected to the process in parallel or series. The parallel connection can be used by attaching the boiler's input and output directly into the buffer tank, as in Fig. 2.4 (a), while a series connection is by installing the boiler directly into the piping system between the process heat and the buffer tank as in Fig. 2.4 (b).

According to the recent literature reviews, two simulations' sets are conducted to optimise the solar system's performance. The first one is to optimise the system performance (considering the solar fraction as the critical factor) for the given characteristics of a solar collector. At the same time, the second type optimises the solar collectors' efficiency. Nevertheless, most of the studies are done using MATLAB or TRNSYS software.

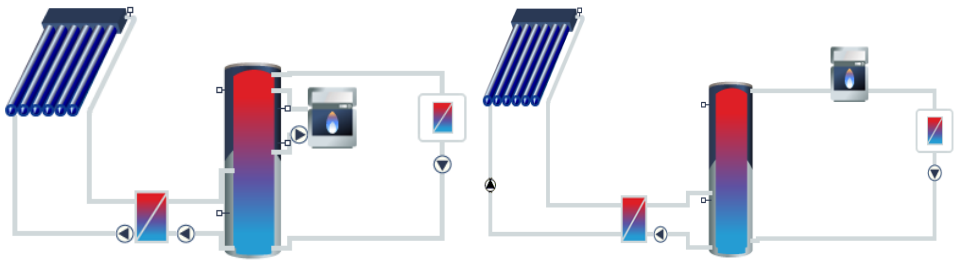

(a) (b)

Fig. 2.4. Solar thermal system for heat process (a) parallel boiler connection (b) series connection

The working profile of a pasteurising plant generally continues during the whole year with short breaks, for example, during Sundays with half working days, Christmas, and summer holidays. The heat process starts every day from 6 AM till 4 PM, starting with the cleaning process at 100% capacity and 90 ℃ or steam compared to 20% capacity and around 73 ℃ for the pasteurising heat process. Indeed, not all pasteurising plants have the same working profiles since they may have different processes, such as cheesing or packaging. However, this study concerns the primary process of all pasteurising plants.

The solar thermal system is simulated using the following parameters:

Different numbers of Evacuated-tube collectors

An Evacuated-tube collector is chosen to choose the optimum collector number with an 87.8% conversion ratio and 1.43 $W/m^2 \cdot K$ and 0.0038 $W/m^2 \cdot K^2$ linear and quadratic heat transfer coefficients. The collector's gross and active areas are 2.14 m^2 and 1.31 $m^{2,}$ respectively, with 8000 $J/m^2 \cdot K$ specific heat capacity.

Collector loop heat exchanger

The maximum heat transferred by the heat exchanger depends on the size of the system. For our study, the mean logarithmic temperature difference (MLTD) is considered at 5 K for all scenarios.

Buffer tank

The buffer tank is an unstratified tank with 100 mm insulation thickness, 0.065 W/m·K thermal conductivity, and an average daily heat loss of 7.10 kWh/day.

Auxiliary heater

53.1 kW gas-fired boiler is connected in parallel with the buffer tank or series with the secondary loop before the process heat section. The boiler's efficiency is 85%, measured based on the low heat value.

Flow circulation pumps

Several pumps are mounted in the system to circulate the running medium fluid. The first is mounted in the primary loop in two places, the first between the solar collector and the external heat exchanger. The second circulates the fluid between the buffer tank and the external heat exchanger. The secondary loop has a circulating pump between the process heat and the buffer tank. For each pump, there is an on/off controlling system that generates the signals for each pump. In the primary loop, the controlling system generates an on signal if the collector’s output temperature is above the tank’s reference temperature by +8 K and an off signal if it is +3 K.

Internal and external piping system

The external piping system is the part between the buffer tank and the solar collectors. At the same time, the internal ones are between the buffer tank and the process heat. The sizing of the pipes is chosen relatively based on 0.5 m/s fluid velocities. A thermal insulator surrounds the piping system with 0.045 W/m·K thermal conductivity and 100% relative thickness to the nominal pipe’s diameter.

Weather and meteorological data

T*sol uses an external weather acquisition program as an external Typical Meteorological Year (TMY) file for the studied location. Budapest is the chosen city in our case study, and the weather data were acquired between 1986 and 2005.

Finally, the RSM method can be done using the five factors abovementioned with both -1 and +1 values, resulting in 5^2 equals 32 experiments and an extra experiment in 0 coded value to illustrate the system linearity or non-linearity as in Table 2.2.

Table 2.2. RSM method coded and real values.

	Coded value		**Real value**	
A – collector area	-1	+1	5 (m^2)	100 (m^2)
B – glycol ratio	-1	+1	5 (%)	80 (%)
C – relative flow rate	-1	+1	5 ($l/h \cdot m^2$)	100 ($l/h \cdot m^2$)
D – relative tank capacity	-1	+1	10 (l/m^2)	100 (l/m^2)
E - tank height-to-diameter ratio	-1	+1	0.2 (m/m)	2.7. (m/m)

3. RESULTS AND DISCUSSION

The experiments' results are presented in this chapter, and the discussions suggest new findings. The solar TES and tankless SHIP mentioned in the previous section were tested in different conditions and working cases in the Hungarian University of Agriculture and Life Sciences lab. The achieved results served as a basis for the new scientific results.

3.1. Experimental results of integrating PCM Soy wax into TES

Based on the R script results, we generated the mathematical second-degree, non-linear, 3-factors interaction equation. Moreover, to generate the second-order coefficients, more experiments were needed. Furthermore, to have a better visualisation, the Pareto plot illustrates the most influential factors of the non-linear equation, where for Soy wax 52℃, the temperature has the most significant positive magnitude, followed by sample and quantity of PCM as in Fig. 3.1. On the contrary, the temperature has the most potent negative magnitude, proving the non-linearity. For Soy wax at 62℃, the second-degree interaction between samples and temperature has the highest positive magnitude, followed by the first-degree temperature effect. In contrast, the three interactions between samples, quantity and temperature have the most extensive negative magnitude. The following equations (3.1 and 3.2) represent the generated models:

$$y_{Soy\ wax\ 52℃} = 9.33 + 0.95(0.5\,S - 3) + 0.38(0.4\,Q - 3) + 3.16(0.2\,T - 7) - 0.38(0.2\,T - 7)^2 + 0.29(0.5\,S - 3)^2 - 0.05(0.5\,S - 3)(0.4\,Q - 3) + 0.23(0.5\,S - 3)(0.2\,T - 7) - 0.11(0.4\,Q - 3)(0.2\,T - 7) - 0.04(0.5\,S - 3)(0.4\,Q - 3)(0.2\,T - 7) \quad (3.1)$$

The 3.1 equation is valid for the Soy wax 52℃ for the following domains:

S ∈ [0-8] samples, Q ∈ [0-10] g, and T ∈ [30 – 60] ℃.

$$y_{Soy\ wax\ 62℃} = 15.03 + 0.84(0.5\,S - 3) + 0.18(0.4\,Q - 3) + 1.62(0.67\,T - 4) - 0.21(0.67\,S - 4)^2 + 0.07(0.4\,Q - 3)(0.5\,S - 3) + 2.04(0.5\,S - 3)(0.67\,T - 4) + 0.85(0.4\,Q - 3)(0.67\,T - 4) - 1.16(0.4\,Q - 3)(0.5\,S - 3)(0.67\,T - 4) \quad (3.2)$$

The 3.2 equation is valid for the Soy wax 62℃ for the following domains:

S ∈ [0-8] samples, Q ∈ [5-10] g, and T ∈ [45 – 75] ℃.

The Pareto plot is conducted to understand the relationship between the factors and the objective, as in Fig. 3.1.

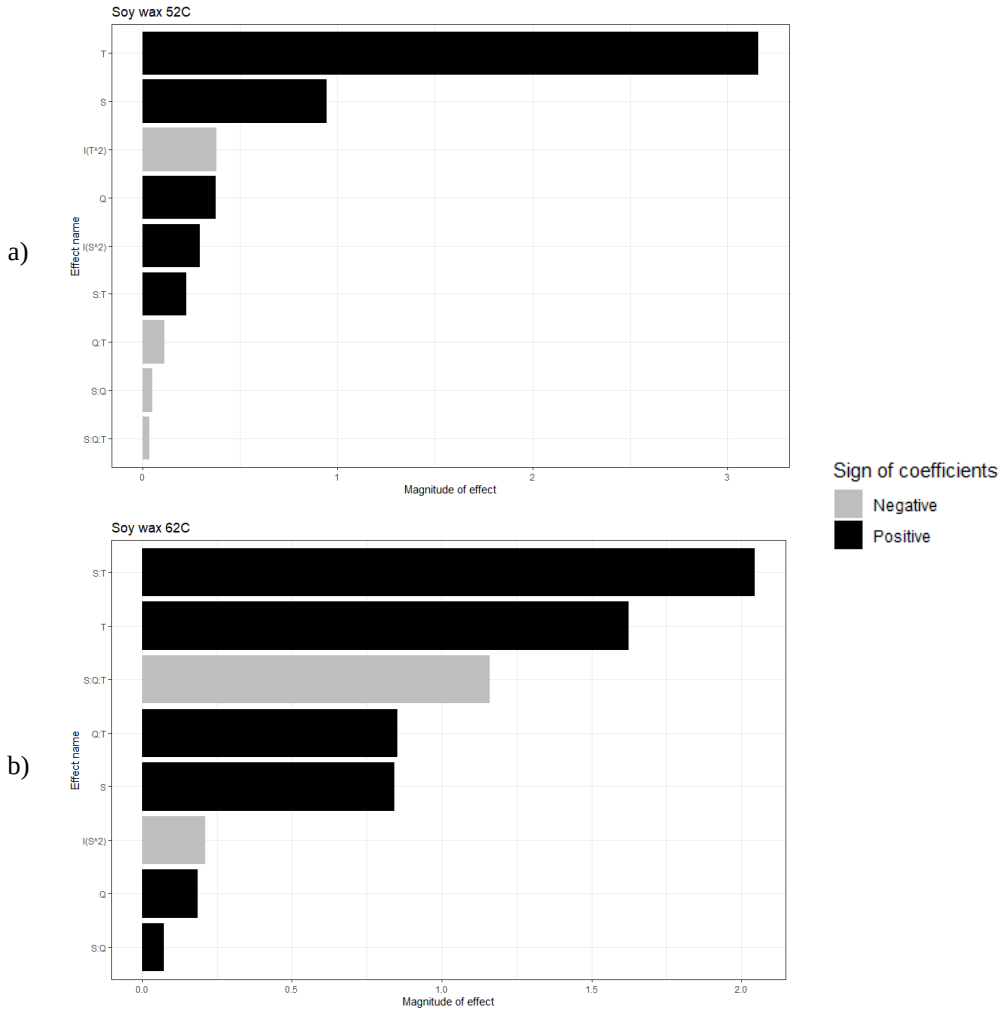

Fig. 31 Pareto plot a) Soy wax 52℃ and b) Soy wax 62℃

S – Samples; Q – Quantity (g); T – Temperature (℃)

3.1.1. Statistical analysis of the soy waxes results

A statistical test was conducted to identify the linearity or non-linearity results significance from the two mathematical models as in equations 3.3 and 3.4. The two equations were tested with and without the two factors' interactions to measure the mean, standard deviation and R^2 values.

Applying the Lagrange multiplier equations to unconstrained optimisation, the objective function y is a function of S, Q, and T as described by equation 3.3. It should be noted that the unconstrained conditions mean no predefined constraints for optimisation.

$$y = y\,(S, Q, T) \tag{3.3}$$

Since there are no conditions for the optimisation, the Lagrange condition for optimum is as in equation 3.4.

$$\nabla y = 0 \tag{3.4}$$

Equation 4.4 can be rewritten as in equation 3.5.

$$\frac{\partial y}{\partial S} = \frac{\partial y}{\partial Q} = \frac{\partial y}{\partial T} = 0 \tag{3.5}$$

By solving the two Soy wax equations 3.1 and 3.2 by deriving them according to S, Q, and T, we get the optimum solutions as in Table 3.1. It should be noted that these two equations were derived once with only first-order factors (linear model) and once with second-order factors included (non-linear model).

Table 3 Optimum values for Soy wax 52℃ and 62℃ using linear and non-linear models

Factors	**Non-linear model**				**linear model**			
	Soy wax 52℃ value		Soy wax 62℃ value		Soy wax 52℃ value		Soy wax 62℃ value	
	Coded	Real	Real	Coded	Coded	Real	Coded	Real
S	-0.090	5.82	3.2809	12.56	4.275	14.55	1.535	9.07
Q	3.587	16.46 g	2.1824	12.956 g	14.74	44.35 g	5.103	20.257 g
T	3.616	53 ℃	0.1385	62.07 ℃	0.592	37.96 ℃	0.3086	64.629 ℃
New y	15.6 (h)		16.36 (h)		15.84 (h)		17.78 (h)	

Concerning the Soy wax 52℃, during the approximation, the coefficients of determination were 99.89% and 99.87% for the nonlinear and linear models, respectively, while the standard deviation was 3.1 for both models. These models represent the closest expression of the relationship between samples, quantity, temperature, and the storage time of the TES.

Consequently, it was proven that the improvement of the storage time using the Lagrange multipliers optimisation process results in 15.6 (h) for the Soy wax 52℃ and 16.36 (h) for the Soy wax 62℃, as shown in Table 3.2 and 3.3.

Table 3 Soya wax 52℃

Non-linear model	***Linear model***
R^2 = 99.99%	R^2 = 94.78%
SD = 4.45 hours	SD = 6.92 hours
t = 15.6 hours	t = 16.36 hours

Table 3 Soya wax 62°C

Non-linear model	Linear model
R^2 = 99.89%	R^2 = 99.87%
SD = 3.1 hours	SD = 3.1 hours
t = 16.36 hours	t = 17.78 hours

3.2. Optimum boiler configurations into SHIP

3.2.1. Required collector area

The modelling for 20 collector areas varies from 5 to 100 m^2 with an incremental step of 5 m^2. Both in-series and parallel systems were modelled while fixing the other variables at 50 l/m^2 tank volume to the solar collector area recommended for solar heat for industrial processes under the climate of central Europe to make the comparison. The relative volume flow rate to each square meter of the collector area is 50 $l/m^2 \cdot h$, as the literature recommends. In the primary loop, the volumetric glycol ratio is 30%. It can stand at -13°C freezing temperature and -30°C for burst protection according to the Hungarian climate. Finally, the height-to-diameter ratio of the buffer tank was chosen to be 1.8 m/m. Above this value, the daily heat losses from the tank will be relatively higher due to the larger exposed surface to the ambient.

As in Fig. 3.2, the results show that, in general, in-series boiler connection has higher results than in parallel configuration. It is noted that the difference reaches its maximum value of 5.8% when the collector area is 65 m^2. At this value, a series connection delivers 65.48% solar fraction while, in parallel, delivers 59.68% only.

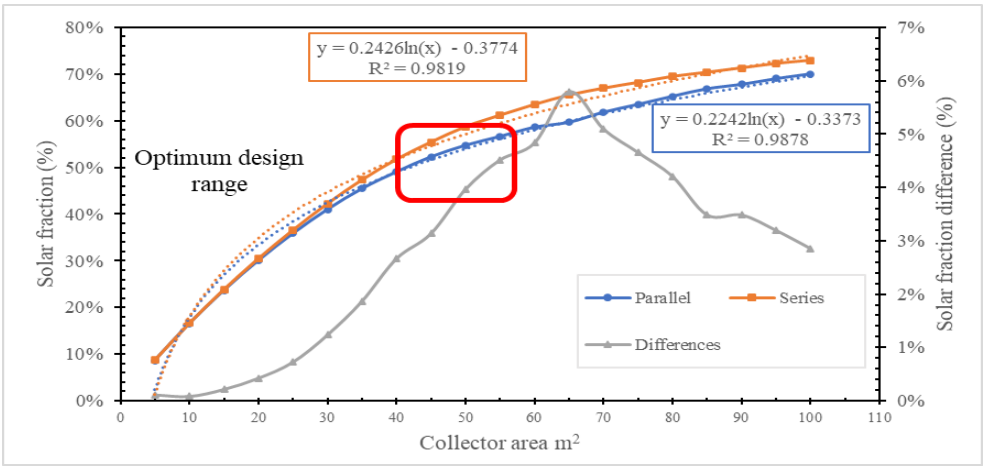

Fig. 3 Collector area versus solar fraction

3.2.2. Glycol ratio configurations

The results show that the series boiler configuration has a higher solar fraction than the parallel one. Nevertheless, the difference does not exceed 0.5% solar fraction at the best scenarios. This concludes that the glycol ratio does not severely affect the solar fraction in both modes, parallel and series. We can say that the glycol ratio does not affect the results from an energetic aspect, but we still have to consider the mechanical and hydraulic aspects.

3.2.3. Collector flow rate configuration

The effect of the relative flow rate in the collector $\frac{\dot{m}}{A_C}$ Varies between 5 to 100 litres/h for each square meter of the gross collector area with an incremental step of 5 l/h·m^2. The results show that an in-series boiler connection generally provides a higher annual solar fraction. The difference in the results is more than 2.05% when the flow rate is 5 l/h·m^2, while it is around 0.5% between 20 – 90 l/h·m^2. According to the recommendation of using 50 l/h·m^2 in the central European climate, the difference is 0.42 – 0.56%.

3.2.4. Relative tank volume configuration

Considered one of the most influential factors in the solar system, relative solar tank volume V_C/A_C is measured at different ratios from 10 to 300 litres buffer tank volume for each collector's gross square meter area as in Fig. 3.3. The results show that, in general, series boiler configurations provide higher solar yield than parallel connections. The maximum difference occurs when V_C/A_C equals 20 litres/m^2 with a 5.1% annual solar fraction difference.

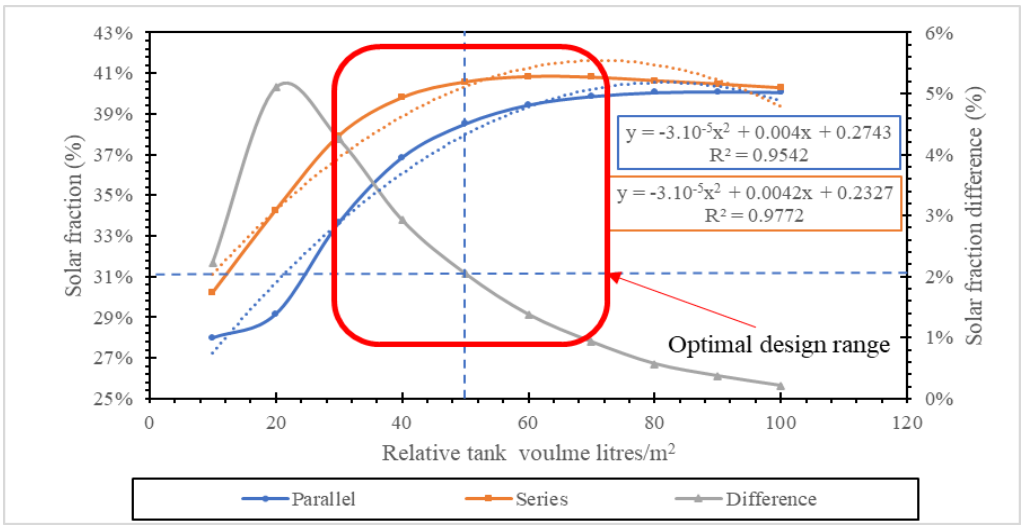

Fig. 3.3.. Relative tank volume effect on the solar fraction

3.2.5. Tank height-to-diameter configuration

Both systems were studied using the tank height-to-diameter ratio as the variable to compare the two configurations. The results show that, in general, a series connection delivers more solar yield than a parallel connection. The variations between the two configurations are 0.44% on average. For recommended designs at a 1.8 m/m tank height-to-diameter ratio, the difference is 0.42% annual solar fraction.

3.2.6. Overall system response to changing factors using RSM method

Many studies consider the final output of their research as one factor changing the result. For example, if the solar collector area changes from 5 to 10 m^2, the solar fraction will increase from 15% to 20%. This argument is not necessarily correct in a real system due to the interaction between the studied factors. According to the same example, changing the collector area will definitely result in extra tank capacity, higher glycol content in the collector loop, and a higher volume flow rate. These facts are explained as follows:

- Generally, we need between 50-75 litres per square meter collector area.
- When having more collectors, we need to have an immense water volume in the collector loop, resulting in larger amounts of glycol.
- When having more collectors, we need a flow rate corresponding to the collector's area, around 75 litres per hour per collector's square area.

It is clear from the parallel system in Fig. 3.4 that factors A, D, and C are the most dominant single factors, while A: D and A: C are the most significant two factors' interactions. The most substantial factor is A, representing the collector area and is times stronger than the other factors, around 28%, while the D factor is 3.15%. This output illustrates that the collector area is critical when planning a solar thermal system, considering the other factors' variations.

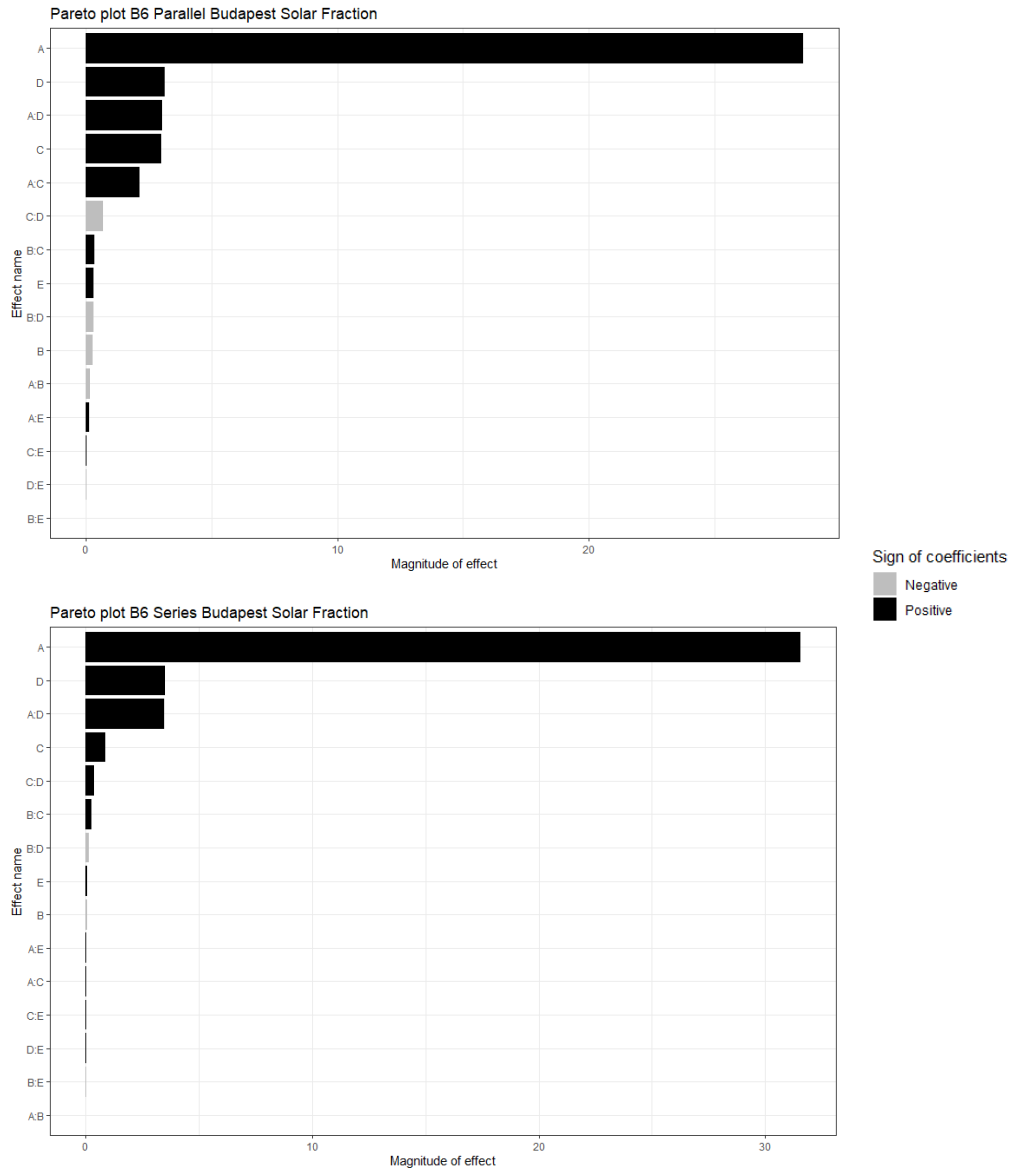

Figure 3.3. Pareto plot for parallel & series boiler configuration solar fraction.

A- Collector area (m^2); B- Glycol ratio (%); C- Relative flow rate ($l/h \cdot m^2$); D- relative tank capacity (l/m^2); E- tank height-to-diameter ratio (m/m).

$$y_{in-Parallel} = 36.60 + 28.53A - 0.26B + 3C + 3.15D + 0.28E - 0.15AB + 2.13AC + 0.32BC + 3.02AD - 0.28BD - 0.7CD + 0.12AE + 0.22ABC - 0.28ABD - 0.72ACD + 0.12ADE \quad (3.6)$$

$$y_{in-Series} = 39.106 + 31.54A + 0.85C + 3.51D + 0.27BC + 3.48AD - 0.13BD + 0.38CD + 0.34ACD \quad (3.7)$$

On the other hand, analysing the RSM results, I noted that the magnitude differences are in the series system's favour. Moreover, comparing the two systems, I found out that in the series system, the set intercept was higher by 3.13%, the A factor by 3.01%, the D factor by 0.37%, and the A: D interaction by 0.47%. On the contrary, the C factor estimate was higher in the parallel system than the series by 2.14% and the A: C interaction was higher by 2.09%. This difference showed that the volume flow rate in the parallel configuration matters because, in a parallel system, both the boiler and the collector loops are parallelly connected to the buffer tank, resulting in no final interference from the boiler into the heat process temperature. For the in-series system, the boiler is connected to the heat process directly before this service, resulting in direct interference from the boiler if the volume flow rate of the collector loop is not suitable. It is also evident from the results that factors B: Glycol ration and E: tank height-to-diameter ratio have very little influence on the overall results.

In conclusion, I proved that in-series boiler configuration provides higher annual solar yields (solar fraction) than in-parallel configuration from the most significant aspects using RSM and analytical methods. On the other hand, the results showed that choosing the RSM method will lead to more actual results than the traditional analytical method, since RSM provide real correlations between the studied factors. In contrast, the analytical method deals with it as independent factors. Due to these results, in-series configurations should be considered when installing solar thermal system technology in industrial plants for a higher outcome and results.

3.3. Tankless SHIP

The outcomes of this research, along with the corresponding physical explanations, are described in this paragraph. Data were collected for the continual flow of hot water at different process heat temperatures, 35 - 60℃ for preheating water and 60 litres per hour configurations of flow rates in the primary and secondary loop and actual solar radiation from the sun.

3.3.1. Hungarian weather profile

A conclusion was drawn to determine the correlation between solar radiation and the ambient temperature from two prospectives: long-term records from 1995 - 2012 and the model results generated by T*sol software. The generated results were without a set intercept meaning (0,0) and linear correlations trendlines. Regarding the long-term records and the modelling, the results show that the correlation between the ambient temperature and solar radiation as in Fig. 3.5 and equations (3.8 and 3.9).

Long-term records:

$$T_{amb} = 0.1456Ra - 7.3775 \text{ where } R^2 = 0.8288 \quad (3.8)$$

Modelling T*sol:

$$T_{amb} = 0.1552Ra - 6.6844 \text{ where } R^2 = 0.8772 \quad (3.9)$$

a)

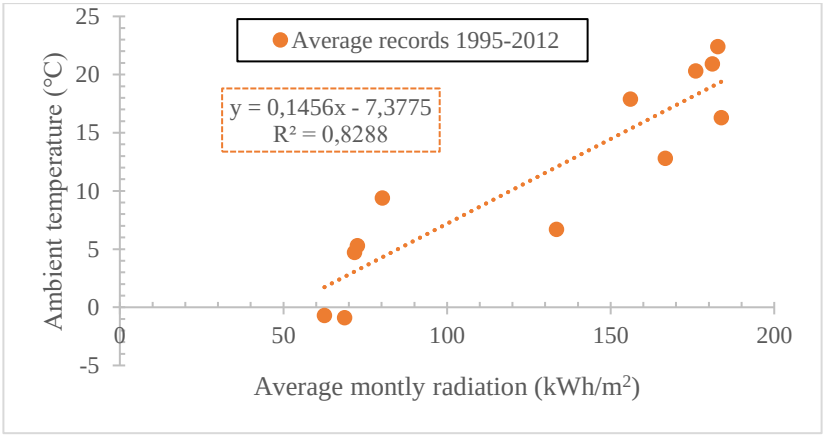

b)

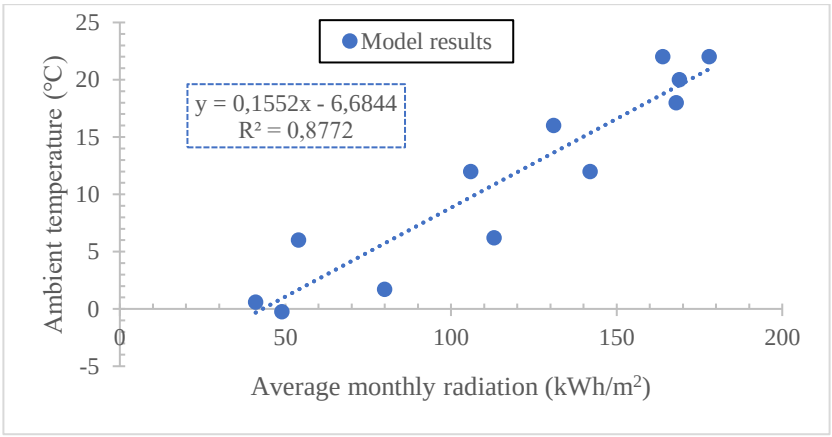

Figure 3 a) Long-term records (1995-2012) and b) T*sol model correlation between the ambient temperature and the solar radiation.

3.3.2. Model validation

The authenticity of the dynamic simulation model using T*sol software of the tankless SHIP has been examined experimentally by real-time measurement for three months at 60/60 litres per hour for both loops (60 l/h primary and 60 l/h secondary). Fig. 3.6 shows the black dashed line, representing the heat process set temperature. It is pretty apparent from the graph that the orange line (representing the secondary output temperature) is always near the set temperature. Hence, the simulation model is appropriate for further predicting system performance. As illustrated, each measurement took place for at least two successive days and was

repeated if necessary due to the unexpected meteorological weather, if applicable. Each measurement's target temperature is set as required for the heat process (HX1_Sec_out), varying from 35 ℃ to 60 ℃.

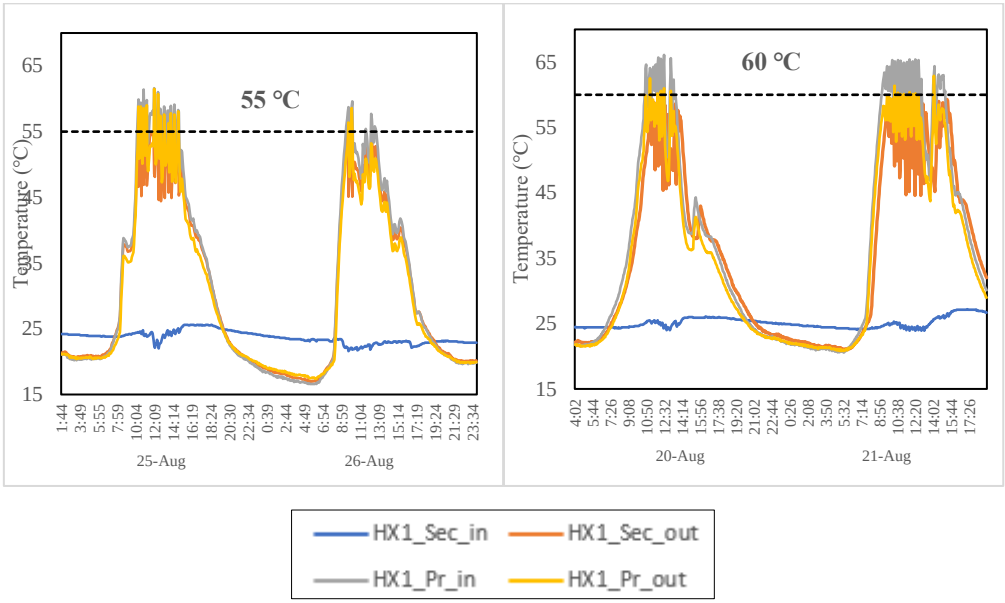

Figure 3 Actual experiments for a different set of output temperatures

HX1_Pr_in - primary input side temperature; HX1_Pr_out - primary output side temperature; HX1_Sec_in - secondary side input temperature; HX1_Sec_out - secondary output side temperature

In addition, the logarithmic mean temperature difference (LMTD) is a tool in flow systems, most notably in heat exchangers, to determine the temperature driving force for the heat transfer process. For a heat exchanger with a specific heat transfer coefficient and constant area, the larger the LMTD the more heat is transferred. For a generic heat exchanger with two ends at which the cold and hot streams enter, the LMTD is defined by equation 3.10:

$$LMTD = \frac{\Delta T_p - \Delta T_s}{\ln\left(\frac{\Delta T_p}{\Delta T_s}\right)} \tag{3.10}$$

On the other hand, the correlation between the LMTD and the specific solar radiation is plotted in Fig. 3.7. It can be seen that for temperature cases 60, 55, and 50 ℃, the correlation between the LMTD and the specific solar radiation on the inclined surface is polynomial from the second order with accelerated increase and set intercept (0,0). At the same time, the 45 ℃ case is a second-degree polynomial correlation with decelerated increase with also set intercept (0,0). On the contrary, 40 and 35 ℃ cases have more linear correlation with a set intercept of (0,0).

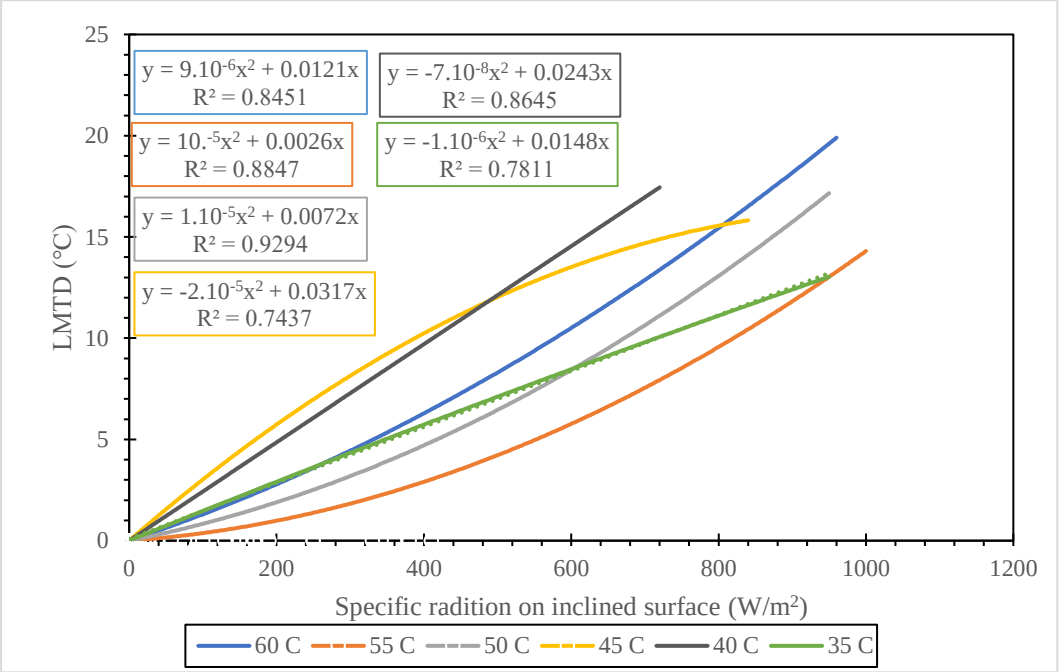

Figure 3 Correlation between LMTD and specific solar radiation on an inclined surface

3.3.3. Parametric analysis

3.3.3.1. Effect of solar radiation and mass flow rate on the outlet temperature

Fig. 3.8 shows the outlet temperature variation under varying solar radiations for three configurations, 30/30, 60/60 and 90/90 litres per hour per square meter mass flow rate. The left-hand side number represents the flow rate at the primary loop, while the right-hand side number represents the secondary loop flow rate. In contrast, the inlet water temperature of the secondary loop was relatively constant at 25℃ return temperature. The modelling was conducted in July 2021, and the results show that the 30/30 configuration has the highest output temperature for summertime compared to 60/60 and 90/90 l/h·m^2. It means obtaining the highest outlet temperature during the summer, 30/30 l/h· m^2 flow rate is the optimum configuration, followed by 60/60 and 90/90, respectively. It was also noted that the linear best-fitting lines are the linear trendlines where the coefficients of determination R^2 were 0.9332, 0.9521 and 0.9384 for configurations 30/30, 60/60, and 90/90, respectively. For example, 800 W/m^2 solar radiation will result in 56℃, 46℃, and 42℃ outlet temperatures for configurations 30/30, 60/60, and 90/90, respectively.

Similarly, higher solar radiation will result in broader temperature ranges between the configurations, while lower solar radiation will result in narrower temperature

ranges. These results explain that when the flow rate is slower in the primary loop, this will allow the glycol-water (1:3) mixture to take more time to absorb the solar radiation from the solar collector and then convey it to the heat exchanger. In addition, the slow flow rate will have lesser friction losses. Finally, it can be concluded that depending on the outlet heat process temperature, the lowest the flow rate, the highest the outlet heat process temperature. These results can be utilised in the solar controlling system to adjust the flow rate at the primary and secondary pumps to obtain the required temperature, as illustrated by equation 3.11:

$$\begin{aligned} &30/30: && T_{out} = 22.611\,\mathrm{Ra} + 23.986; && R^2 = 0.9332 \\ &60/60: && T_{out} = 28.248\,\mathrm{Ra} + 22.811; && R^2 = 0.9384 \\ &90/90: && T_{out} = 40.615\,\mathrm{Ra} + 22.194; && R^2 = 0.9521 \end{aligned} \quad (3.11)$$

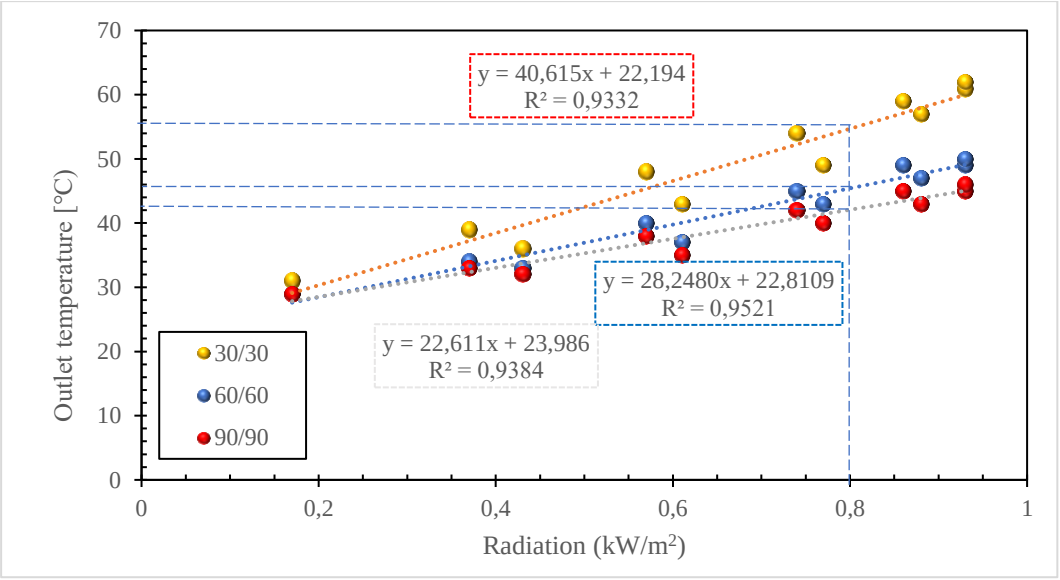

Figure 3.8. Effect of solar radiation on water outlet temperature for tankless SHIP system at different flow rates

3.3.3.2. Effect of solar gain under different mass flow rate

Fig. 3.9. illustrates the variation of the generated thermal energy fraction from the tankless SHIP system for the specific industrial process under varying solar radiation and mass flow rates. The annual energy yield represents the valuable energy harvested by one square meter of the solar collector and transported through the primary loop. Results show that the 30/90 configuration has the highest annual energy yield of 638.79 kWh/m^2. In other words, one square meter of the collector area generates 638.79 kWh per year. Similarly, the 30/60 and 60/90 configurations have 621.5 and 604.05 kWh/m^2 annual energy yield,

respectively. The remaining configurations have less than 600 kWh/m^2 annual energy yield. It is noted from the graph that the second loop must have a higher flow rate compared to the primary loop, which is a result of choosing a closed loop on the primary side. At the same time, the open loop on the secondary side shows that a higher flow rate results in higher yields if we consider a fixed flow rate at the primary loop.

Using the R script, the annual energy gain can be generated using the primary and secondary flow rates with coded values -1 equals 30 litres per hour and +1 equals 90 litres per hour. As a result, 0 coded values will be 60 litres per hour. The following equation 3.12 represents the generated formula knowing that R^2 equals 0.9128:

$$E = 577.598 + 41.663\ Q_{pr} - 24.717\ Q_{sec} + 1.422\ Q_{pr}\ Q_{sec} \qquad (3.12)$$

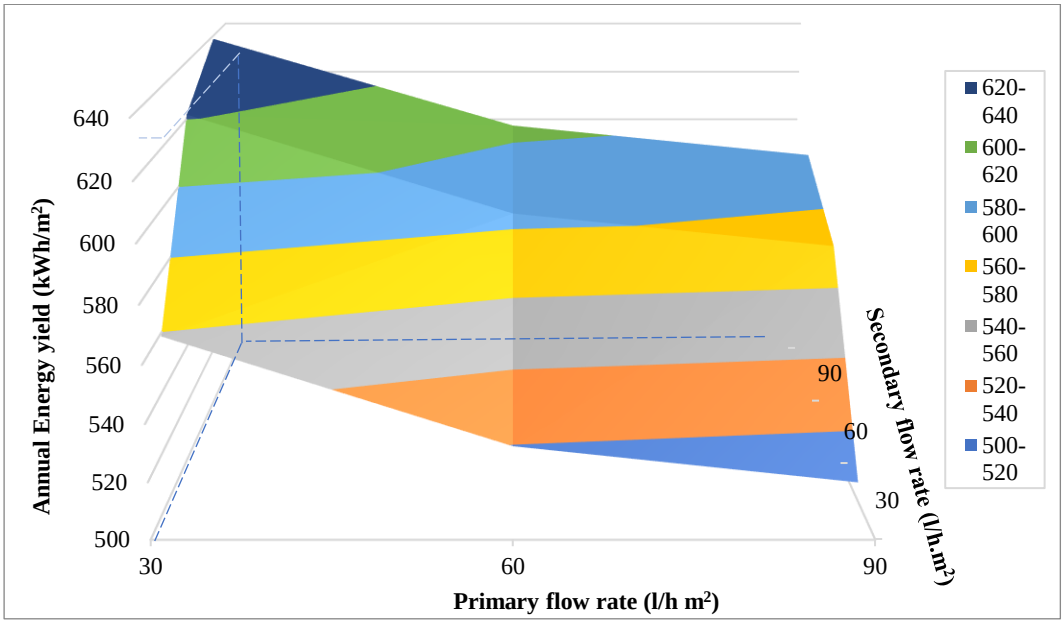

Figure 3 Annual energy yield considering different flow rate configurations

4. NEW SCIENTIFIC RESULTS

The results were comprehensively investigated in this study, and the following points are noteworthy to be mentioned:

4.1. Correlation between the phase change material Soy wax integrated into the Thermal Energy Storage

Based on the experimental results, I enhanced the solar thermal tank's storage time by integrating two types of Soy wax at two melting temperatures, 52℃ and 62℃. To justify this enhancement, I developed a non-linear model that can be applied to TES operating solar buffer tanks using encapsulated PCMs and considering the most influential factors, wax quantity (Q), sample quantity (S), and temperature (T). The Equations 4.1 and 4.2 represent the mathematical correlation using actual values:

$$y_{Soy\ wax\ 52℃} = 9.33 + 0.95(0.5\,S - 3) + 0.38(0.4\,Q - 3) + 3.16(0.2\,T - 7) - 0.38(0.2\,T - 7)^2 + 0.29(0.5\,S - 3)^2 - 0.05(0.5\,S - 3)(0.4\,Q - 3) + 0.23(0.5\,S - 3)(0.2\,T - 7) - 0.11(0.4\,Q - 3)(0.2\,T - 7) - 0.04(0.5\,S - 3)(0.4\,Q - 3)(0.2\,T - 7) \quad \text{(hour)};$$

$$R^2 = 99.99\%; \qquad SD = 4.45 \text{ hours} \tag{4.1}$$

The 4.1 equation is valid for the Soy wax 52℃ for the following domains:

S ∈ [0-8] samples, Q ∈ [0-10] g, and T ∈ [30 – 60] ℃.

$$y_{Soy\ wax\ 62℃} = 15.03 + 0.84(0.5\,S - 3) + 0.18(0.4\,Q - 3) + 1.62(0.67\,T - 4) - 0.21(0.67\,S - 4)^2 + 0.07(0.4\,Q - 3)(0.5\,S - 3) + 2.04(0.5\,S - 3)(0.67\,T - 4) + 0.85(0.4\,Q - 3) * (0.67\,T - 4) - 1.16(0.4\,Q - 3)(0.5\,S - 3)(0.67\,T - 4) \quad \text{(hour)};$$

$$R^2 = 99.89\%; \qquad SD = 3.1 \text{ hours} \tag{4.2}$$

The 4.2 equation is valid for the Soy wax 62℃ for the following domains:

S ∈ [0-8] samples, Q ∈ [5-10] g, and T ∈ [45 – 75] ℃.

By applying the Lagrange multiplier method $\mathbf{y = y\,(S, Q, T)}$ using unconstrained optimisation $\boldsymbol{\nabla\, y = 0}$, I identified the optimum values for operating factors as in Equations 4.3 and 4.4:

S = 5.82 samples, Q = 16.46 g, and T = 53 ℃ for Soy wax 52℃

$$\rightarrow y_{Soy\ wax\ 52℃} = 15.6 \text{ (h)} \tag{4.3}$$

S = 12.56 samples, Q = 12.956 g, and T = 62.07 ℃ for Soy wax 62℃

$$\rightarrow y_{Soy\ wax\ 62℃} = 16.3 \text{ (h)} \tag{4.4}$$

4.2. Correlation between the solar fraction and the boiler configurations in the solar heat for industrial prcesses

Based on the analytical results, I proved that the in-series configuration is the most efficient and productive one to get the highest solar fraction. I have pointed out that the collector area, relative flow rate, and relative tank volume have a tangible influence on the overall yield. In contrast, the glycol and tank height-to-diameter ratios have a lesser impact. It is essential to mention that the targeted solar fraction domain is between 40 – 60% since lower than this value, the solar thermal system will not be effective and higher than this will not be feasible. Considering the analytical method, I calculated the solar fraction as a function of collector area A and relative tank volume D as in equations 4.5 and 4.6, valid for A ∈ [5-100] m^2 and D ∈ [5-100] litres/m^2:

$$\left.\begin{aligned} y_{in-series} &= 0.2426\ \ln(A) - 0.3774 \quad (\%); \qquad R^2 = 0.9819 \\ y_{in-parallel} &= 0.2242\ \ln(A) - 0.3371 \quad (\%); \qquad R^2 = 0.9878 \end{aligned}\right\} \quad (4.5)$$

$$\left.\begin{aligned} y_{in-series} &= -3.10^{-5}\ D^2 + 0.0042\ D + 0.2327 \quad (\%);\ R^2 = 0.9772 \\ y_{in-parallel} &= -3.10^{-5}\ D^2 + 0.0040\ D + 0.2743 \quad (\%)\ ;\ R^2 = 0.9542 \end{aligned}\right\} \quad (4.6)$$

While for the RSM method, the formula concerning the solar fraction in (%) unit concludes both factors: solar collector area, relative tank capacity, and their two-factor interaction as in equation 4.7 which are valid for A ∈ [5-100] m^2 and D ∈ [5-100] litres/m^2 as follow:

$$\left.\begin{aligned} y_{in-Parallel} &= 36.60 + 28.53\left(\frac{A-52.5}{47.5}\right) + 3.15\left(\frac{D-55}{45}\right) + 3.02\left(\frac{A-52.5}{47.5}\right) * \left(\frac{D-55}{4}\right)\ (\%) \\ y_{in-Series} &= 39.11 + 31.54\left(\frac{A-52.5}{47.5}\right) + 3.51\left(\frac{D-55}{45}\right) + 3.48\left(\frac{A-52.5}{47.5}\right) * \left(\frac{D-55}{4}\right) \quad (\%) \end{aligned}\right\} \quad (4.7)$$

4.3. Tankless solar heat for industrial process system validation

I experimentally examined the authenticity of the dynamic simulation model using T*sol software of the tankless SHIP by real-time measurement for three months of the experiment at 60 litres per hour for both the primary and secondary loops. Firstly, I have found minimal deviation between my measured meterological data (for one year) and the applied model (data from 1995 - 2012), so my model is applicable well in practice. Furthermore, the following two equations represent the correlation between the monthly average solar radiation values and the ambient temperature for both the model, equation 4.8, and the long-term records, valid for T_{amb} ∈ [0 – 25] °C and Ra ∈ [0 – 1000] W/m^2, 1.92 m^2 and 33º inclined FPC, and 960 W Alfalaval heat exchanger.

$$\left.\begin{aligned} &\text{Long-term records: } T_{amb} = 0.1456\ Ra - 7.3775\ (°C);\ \text{where } R^2 = 0.8288 \\ &\text{Modelling T*sol: } \quad T_{amb} = 0.1552\ Ra - 6.6844\ (°C);\ \text{where } R^2 = 0.8772 \end{aligned}\right\} \quad (4.8)$$

I also calculated the correlation between the simplified model LMTD efficiency indicator and the specific solar radiation of the inclined surface using six different temperature targets (35 – 60℃). The results show using a set intercept of (0,0) that for temperature cases 50, 55, and 60℃, the correlation is a second-degree polynomial correlation with accelerated increase. In contrast, case 45℃ is a second-degree polynomial with a decelerated increase. On the contrary, cases 40 and 35℃ showed a linear correlation with set intercept (0,0). The set Equation 4.9 shows the correlations for all cases with the appropriate trendline.

$$\begin{aligned}
&60℃; \quad LMTD = 9.\,10^{-6}\,Ra^2 + 0.012\,Ra; && R^2 = 0.8451\\
&55℃; \quad LMTD = 10^{-5}\,Ra^2 + 0.0026\,Ra; && R^2 = 0.8847\\
&50℃; \quad LMTD = -10^{-5}\,Ra^2 + 0.0072\,Ra; && R^2 = 0.9294\\
&45℃; \quad LMTD = -2.\,10^{-5}\,Ra^2 + 0.0317\,Ra; && R^2 = 0.7437\\
&40℃; \quad LMTD = -7.10^{-8}\,Ra^2 + 0.0243\,Ra; && R^2 = 0.8628\\
&35℃; \quad LMTD = -1.10^{-6}\,Ra^2 + 0.0148\,Ra; && R^2 = 0.7811
\end{aligned} \qquad (4.9)$$

4.4. The effect of solar radiation and mass flow rate on the solar heat for industrial process outlet temperature

For identifying the optimum flow rate in the primary and secondary loops of the solar heat for industrial process system, I calculated the outlet temperature variation under varying solar radiations for three different configurations, 30/30, 60/60 and 90/90 litres per hour per square meter mass flow rate. In contrast, the inlet water temperature of the secondary loop was relatively constant at 25℃ return temperature. The experiment was conducted in July, and the results show that the 30/30 configuration has the highest output temperature for summertime compared to 60/60 and 90/90 l/h m^2. This result highlights that the lowest possible flow rate is the best for having the highest possible outlet temperature since the water-glycol mixture will have a longer time absorbing the energy from the collector loop and then transfer it to the heat process. I identified the relationship between the rendition in (kWh/m^2) and the outlet temperature in Celsius degrees (℃) and the coefficient of determination R^2 as in Equations 4.10, 4.11, and 4.12:

$$T_{out} = 40.615\,Ra + 22.194\ (℃)\ ;\ R^2 = 0{,}9332 \quad 30\ litre/hour \cdot m^2;\ \text{if } T_{in} = 25℃ = const. \qquad (4.10)$$

$$T_{out} = 28.248\,Ra + 22.811\ (℃)\ ;\ R^2 = 0{,}9521 \quad 60\ litre/hour \cdot m^2;\ \text{if } T_{in} = 25℃ = const. \qquad (4.11)$$

$$T_{out} = 22.611\,Ra + 23.986\ (℃);\ R^2 = 0{,}9384 \quad 90\ litre/hour \cdot m^2;\ \text{if } T_{in} = 25℃ = const. \qquad (4.12)$$

4.5. The impact of solar gain under different mass flow rates

I illustrated the variation of the generated thermal energy gain from the tankless SHIP system for the specific industrial process under varying solar radiation and mass flow rates. I noticed that the 30 (l/h·m^2) for the primary loop and 90 (l/h·m^2) for the heat process loop configuration has the highest annual energy yield of 638.79 kWh/m^2. Similarly, the 30/60 and 60/90 configurations have 621.5 and 604.05 kWh/m^2 annual energy yield, respectively. I also noted from the graph that the second loop must have a higher flow rate than the primary loop, resulting in choosing a closed loop on the primary side as a favourable configuration. At the same time, the open loop on the secondary side shows that a higher flow rate results in higher yields if we consider a fixed flow rate at the primary loop. The boundary conditions were the secondary inlet water temperature (T_{Sec_In} = 25°C) was constant, the three selected specific primary/secondary mass flow rates were 30/30, 60/60 and 90/90 (litres/hour·m^2), water/glycol ratio (1:3) and solar radiation interpretation range 0.2 - 0.9 (kW/m^2).

The annual energy gain can be generated using the R script's primary and secondary flow rates when the coded values -1 equals 30 litres per hour, and +1 equals 90 litres per hour. As a result, 0 coded values will be 60 litres per hour. The following equation 4.13 represents the generated formula, knowing that this equation is valid for primary and secondary flow rates range (30 – 90) litres/hour·m^2:

$$E = 577.598 + 41.663.\left(\frac{Q_{pr}-60}{30}\right) - 24.717.\left(\frac{Q_{sec}-60}{30}\right) \quad \text{(kWh/year);}$$

$$R^2 = 0.9128 \qquad (4.13)$$

5. CONCLUSION AND SUGGESTIONS

In conclusion, a dynamic experimental and modelling investigation has been carried out of various types of solar thermal systems for industrial heat process objectives. A comparison between Soy wax 52℃ and 62℃ has studied the effect of integrating encapsulated specimens of PCMs into solar TES to extend the storage time and the thermal efficiency. Each experiment generates eight cases, and supplementary interior or exterior cases were used to rectify the contour lines using the RSM approach and R script coding. The results showed that non-linear behaviour is the best fit considering the most influential factors (wax quantity, sample quantity, and temperature). Both waxes showed in the Pareto plots that the temperature factor is the most substantial single factor magnitude, followed by samples and quantity. In contrast, the second-degree factors showed that temperature and samples are crucial for Soy wax 52℃ and the sample factor for Soy wax 62℃. Also, the two factors' interactions were illustrated using contour plots, and the S · T interaction is the most influential for both experiments. Then, the optimum operating values of both experiments were identified using the Lagrange multiplier method with unconstrained boundary conditions. Using the values will result in 15.6 (h) and 16.36 (h) for Soy wax 52℃ and 62℃, respectively.

The mechanical configuration of the solar heat for industrial processes significantly improves the solar fraction and system efficiency. The boiler can be connected to the heat process in series or parallel. The results were analysed using analytical and dynamic approaches. Both approaches showed that in-series configuration delivers higher solar fraction than in-parallel one. The studied factors are collector area, glycol ratio, relative tank volume, relative volume flow rate and tank height-to-diameter ratio. Analytically, collector area and relative tank volume are the most critical factors considering the optimum design of 40 - 60% solar fraction. On the other hand, RSM approaches showed that in-parallel configuration collector area, relative flow rate, and relative tank capacity are the most significant single factors. At the same time, the interaction of the collector area with relative tank capacity and collector area with relative flow rate are the most crucial two-factor interactions. The same applies to in-series configuration, except that relative flow rate has no significant influence on the overall solar fraction. It was concluded that the RSM approach gives more realistic and dynamic results than the analytical method.

The real-time measurement of the tankless SHIP compared to the dynamic simulation model was examined for three months at 60 litres per hour for both primary and secondary loops. Targeted temperatures (35 - 60℃) could be

approached using the tankless SHIP during the measurement time for all target sets of the heat process. Also, the heat exchanger efficiency passing the heat from the primary side to the secondary one was conducted as a linear correlation with (0,0) set intercept. For all scenarios, the coefficient of determination was consistently higher than 98.63%, illustrating that the difference between the primary side inlet temperature and the secondary side outlet temperature is as minimum as possible. Similarly, the heat exchanger LMTD values were correlated with the specific solar radiation on the inclined surface using a second-degree polynomial correlation trendlines.

To evaluate the SHIP outlet temperature as a relationship between the solar radiation and the mass flow rate, three configurations, 30/30, 60/60 and 90/90 litres per hour per collector's square area, were calculated. The experiment showed that the 30/30 configuration has the highest output temperature. In addition, the formula connecting the solar radiation (kWh/m^2) with the output temperature (°C) was generated with a 93.32% coefficient of determination. In contrast, the 30/90 configuration has the highest annual energy yield of 638.79 (kWh/m^2). It is noted that the secondary loop must have a higher flow rate than the primary one.

This topic is fertile for further exploration since many aspects remain uncovered. To highlight some of the numerous recommendations, for example, the solar thermal heat processes can be tested using other simulations like MATLAB and ANSYS. Also, other types of solar collectors can be evaluated to improve the solar fraction, like black chrome FPC, FPC with selenium coating, and unglazed collectors. In addition, other types of integrated or encapsulated cheap PCMs can be tested to improve the TES or the solar collector. The solar thermal process can also be tested at a higher temperature for medium-temperature industrial processes.

6. SUMMARY

In this work, a comprehensive experimental and modelling investigation was carried out to evaluate solar heat's energetic and thermal performance for industrial process systems. The studied system consists of several parts: solar collector, storage tank, heat exchangers, boiler, and hydraulic system. The storage tank has been analysed to improve the storage time by integrating encapsulated PCMs Soy wax 52℃ and 62℃ into an 8.7 litre 42 x 13 x 16 (cm) storage tank. The tank is well insulated by 5 cm of expanded polystyrene (EPS) material, and the specimen tray comprises 7 x 3 specimens, each holding up to 50 mL of the PCM material. The most influential factors (sample quantity, samples, and temperature) have been analysed, generating $3^2 = 8$ experiments for each PCM (3- factors, 2-cases/factor) and supplementary interior and exterior experiments to rectify the contour lines. The used approach is RSM to identify the single and two-factor magnitudes using Pareto plots and contour lines, while R script was used for coding. The results showed different intercept values, 9.33 (h) and 15.03 (h), for Soy wax 52℃ and 62℃, respectively. In addition, temperature, samples, and quantity are the most influential factors, and its magnitudes for Soy wax 52℃ are higher than 62℃. On the contrary, samples and temperature have substantial second-degree magnitude on Soy wax 52℃ while only samples on Soy wax 62℃. It was noted that the non-linear behaviour is the best-fit solution for the two waxes with 99.99% and 99.89% coefficient of determination for Soy wax 52℃ and 62℃, respectively. The equations generated from the RSM process were used for obtaining the optimum parameters using a Lagrange multiplier with unconstrained boundary conditions. The results showed 15.6 and 16.36 (h) storing time for Soy wax 52℃ and 62℃, respectively.

A different aspect of the hydraulic configuration of the boiler was tested under two different conditions: in series and parallel. The boiler is an essential part of the solar thermal system, and the optimum configuration will result in higher solar fraction yield. Analytical and RSM approaches were used, and the five most important factors were analysed: collector area, glycol ratio, relative flow rate, relative tank capacity, and tank height-to-diameter ratio. Analytically and using the RSM method, collector area and relative tank capacity significantly impact the solar fraction on in-series configuration. In contrast, the RSM method showed that the relative flow rate has a magnitude of the in-parallel configuration. For two-factor interactions, the collector area with relative tank capacity has significant magnitude on both configurations and the collector area with relative flow rate only on in-parallel configuration.

Real-time measurement of the tankless SHIP took place for the whole summer with dynamic simulation models at 60 ($l/h \cdot m^2$) relative flow rate for primary and secondary loops. The experiments targeted several sets of outlet heat process temperatures for low-temperature industrial duties under Hungarian weather conditions, and all the temperature targets were reached. In addition, the heat exchanger efficiency was tested with a linear correlation using (0,0) set intercept with a 98.63% R^2 coefficient of determination. Similarly, the LMTD values were measured, and all scenarios showed more than eight, representing the high efficiency of the heat exchanger. Moreover, the correleation between the LMTD and the specific solar radiation on the inclined surface was drawn for all cases.

The heat process temperature due to the solar radiation and mass flow rate at different configurations was also estimated, showing that 30/30 ($l/h \cdot m^2$) is the optimum value. In contrast, while considering the highest annual energy, the 30/90 ($l/h \cdot m^2$) configuration can yield 638.79 (kWh/m^2) with a 93.32% coefficient of determination.

7. ÖSSZEFOGLALÁS (SUMMARY IN HUNGARIAN)

Ebben a munkámban átfogó kísérleti és modellezési vizsgálatokat végeztem a napenergia termikus teljesítményének értékelésére vonatkozóan, iparban alkalmazott rendszerek esetében. Az általam vizsgált rendszer több részegységből épült fel: napkollektor, tárolótartály, hőcserélő, kazán és a hidraulikai rendszer. A tárolási idő javítása érdekében elemeztem, hogy ha egy 8,7 literes, 42x13x16(cm) méretű tárolótartályba (52°C és 62°C-os olvadáspontú) szója viasz kapszulákat teszek, hogyan változik a tárolási idő, a különböző beállítások esetén. A tartály jól szigetelt 5 cm-es expandált polisztirol (EPS) anyaggal lett bevonva, a minta tartó tálcába 7x3db mintát helyeztem, amelyek mindegyike legfeljebb 50ml fázisváltó anyagot (PCM) tartalmazott. A kísérleti faktorok hatásainak vizsgálatára RSM (válaszfelületi-módszert) módszert alkalmaztam. Pareto-elemzés segítségével azonosítottam a legjelentősebb tényezőket, melyek befolyásolják a folyamatomat. R-script programot használtam a kódolt adatok feldolgozásához. A legjelentősebb tényezőket, a minta mennyiséget (Q), a minta darabszámát (S), a hőmérsékletet (T) változtattam és kísérleti eredmények alapján elemeztem a megkapott adatokat (52°C és 62°C-os olvadáspontú) szója viasz alkalmazása esetén. Az eredmények különböző értékeket mutattak, 9,33(h) és 15,03(h), a szójaviasz 52°C és 62°C esetében. Megállapítottam, hogy nem lineáris az összefüggés a két viasz esetében a három legjelentősebb tényező figyelembevétele esetén. A legjobban illeszkedő egyenletek a két szójaviasz esetében, 99,99%-os és 99,89%-os együtthatóval rendelkeztek. Az RSM-folyamatból generált egyenleteket “Lagrange multiplier” módszerrel az optimális paraméterek meghatározására használtam, és az eredmények 15,6 és 16,36 (h) tárolási időt mutattak a szójaviasz 52°C és 62°C esetében.

A napkollektoros rendszerekben is előszeretettel alkalmazott kazán hidraulikai konfigurációjának különböző összeállítását vizsgáltam: soros és párhuzamos. Az optimális konfiguráció kiválasztása nagyobb szoláris frakcióhozamot eredményez. Két megközelítést alkalmaztam, analitikus és RSM módszert, és az öt legfontosabb tényezőt elemeztem: kollektor felület, glikol arány, relatív áramlási sebesség, relatív tartálykapacitás és a tartály magasság és átmérő arány. Az RSM-módszerrel megállapítottam, hogy a kollektor felülete és a relatív tartálykapacitás jelentősen befolyásolja a szoláris frakció alakulását a soros konfiguráció esetén. Ezzel szemben ugyancsak az RSM-módszer azt mutatta, hogy a relatív áramlási sebességnek van nagyobb hatása a párhuzamos konfiguráció esetén. Ugyanakkor a kéttényezős kölcsönhatások esetében a kollektor felülete a relatív tartálykapacitással együttes hatása mindkét

konfigurációnál jelentős, a kollektor felülete a relatív áramlási sebességgel együtt már csak a párhuzamos konfigurációnál jelentős.

A vizsgálataim során a tartály nélküli kollektoros rendszer valós idejű mérésével validáltam az általam felállított dinamikus szimulációs modelleket ismert relatív áramlási sebesség alkalmazása esetén, 2021. év nyár folyamán. A kísérletek magyarországi időjárási körülmények között történtek, alacsony hőmérsékletű ipari feladatokhoz szükséges kimeneti hőmérséklet előállítását céloztam meg. Megállapítottam több solar radiation és LMTD (logaritmikus átalgos hőmérséklet-különbség) összefüggést különböző kívánt technológiai kimeneti hőmérséklet esetére, sík kollektor alkalmazásával. Az általam megfogalmazott összefüggések 0,8-0,9 korrelációs együthatókat mutattak.

A lemezes hőcserélő primer és szerkunder körében beállított tömegáramok alapján megállapítottam összefüggéseket, mellyel a global sugárzás ismeretében a technológiához szükséges hőmérsékletet lehet meghatározni.

Meghatároztam egy éves energiamennyiség összefüggését a primer és szekunder térfogatáramok függvényében.

A2: Publications related to the dissertation

Refereed papers in foreign languages:

1. **Ghabour, R.**, Korzenszky, P. (2020): Mathematical modelling and experimentation of soy wax PCM solar tank using response surface method, *Analecta Tech. Szeged*, 14 (2), 35–42, ISSN: 2064-7964, https://doi.org/10.14232/analecta.2020.2.35-42.
2. **Ghabour, R.**, Josimović, L., Korzenszky, P. (2021): Two analytical methods for optimising solar process heat system in pasteurising plant, *Applied Engineering Letters*, 6, 166–174, 2021, ISSN: 2466-4847. https://doi.org/10.18485/aeletters.2021.6.4.4, (Scopus: Q3).
3. **Ghabour, R.**, Korzenszky, P. (2021): Technical and non-technical difficulties in solar heat for industrial process. *ACTA Tech CORVINIENSIS – Bulletin of Engineering*, 3, 11–8, ISSN: 2067-3809, https://acta.fih.upt.ro/pdf/archive/ACTA-2021-3.pdf.
4. **Ghabour, R.**, Korzenszky, P. (2021): Effect of series and parallel flow heater configuration of industrial solar heat processes, *Science, technology and innovation*, 14 (3), 18-26, 2021, ISSN: 2544-9125, https://doi.org/10.55225/sti.315.
5. **Ghabour, R.**, Korzenszky, P. (2021): Identifying the optimum tilting angles for solar thermal collectors using four different modelling factors in Hungary. *Hungarian agriculture research*.,21, 51-64, ISSN: 2060-3789.
6. **Ghabour, R.**, Korzenszky, P. (2021): Optimal design and configuration for pasteurizing heat demand supported by solar thermal system using T * sol, ANNALS of faculty engineering Hunedoara – International journal of engineering, 2, 105-110, ISSN: 2601-2332, https://annals.fih.upt.ro/pdf-full/2022/ANNALS-2022-2-16.pdf.
7. **Ghabour, R.**, Korzenszky, P. (2021) Assessment and Modelling of Industrial-Scale Solar Thermal System Application in Hungary. *Hungarian Agriculture Engineering*, 40, 70-77, ISSN: 2415-9751, https://doi.org/10.17676/HAE.2021.40.70.
8. **Ghabour, R.**, Korzenszky, P. (2022): Economic and energetic assessment of industrial-scale solar thermal energy in the Visegrád region, *Analecta Technica Szegedinensia*, 17 (1), 1-9, ISSN: 2064-7964, https://doi.org/10.14232/analecta.2023.1.1-9.
9. **Ghabour, R.**, Korzenszky, P. (2022): Feasibility study of using solar thermal energy for heating swimming pools in central European climate (Hungary as a case study), *Hungarian Agriculture engineering*, 41, 72-78, ISSN: 2415-9751, https://doi.org/10.17676/HAE.2022.41.72.

10. **Ghabour, R.,** Korzenszky, P. (2022): Linear Model of DHW System Using Response Surface Method Approach**,** Tehnički *vjesnik*, 29 (1), 66-72, ISSN: 1848-6339, https://doi.org/10.17559/TV-20201128095138, (IF: 0,783; Scopus: Q2).
11. **Ghabour, R.**, Korzenszky, P. (2022): Dynamic modelling and experimental analysis of tankless solar heat process system for preheating water in the food industry, *Acta polytechnica Hungarica*, 20 (4), 65-83, ISSN: 1785-8860, (IF: 1.806; Scopus: Q2).

International conference abstracts:

12. **Ghabour, R.**, Korzenszky, P. (2018): Studying the possibility of providing the thermal requirements of pasteurization by PV/T solar system in Hungary, *International Conference on Science, Technology, Engineering and Economy*: ICOSTEE 2018: Book of Abstracts Szeged, Hungary: University of Szeged Faculty of Engineering (2018) pp. 20, ISBN:9789633066201.
13. **Ghabour, R.**, Korzenszky, P. (2018): Study of renewable energies within the industrial sector in Hungary: energetic and economic analysis, *Tudományos Diákköri Konferencia előadásainak összefoglalói 2018* Gödöllő, Hungary: Szent István Egyetemi Kiadó (2018) pp. 48, ISBN: 9789632697857.
14. **Ghabour, R.**, Korzenszky, P. (2019): Optimum solar thermal energy utilization in food industry: case study of a dairy plant, *SYNERGY - Engineering, Agriculture and Green Industry Innovation*: ABSTRACTS of the VI. International Conference of CIGR Hungarian National Committee and the Szent István University, Faculty of Mechanical Engineering and the XXXIX. R&D Conference of Hungarian Academy of Sciences, Committee of Agricultural and Biosystems Engineering, Gödöllő, Hungary, pp. 22. November 2019. Gödöllő, Hungary: Szent István University Faculty of Mechanical Engineering, ISBN: 9789632698540.
15. **Ghabour, R.**, Korzenszky, P. (2021): Effect of in-series and in-parallel flow heater configuration of solar heat system for industrial processes, *Risk Factors of Food Chain*: XXIst International Conference: Book of abstract Iwonicz, Poland: Uniwersytet Rzeszowski (2021) pp. 15, ISBN:9788379969326.
16. **Ghabour, R.**, Korzenszky, P. (2021): Mathematical modelling and experimentation of Soy wax PCM solar tank using response surface method, *XXIV. Tavaszi Szél Konferencia (2021)*: Absztrakt kötet Budapest, Hungary: Association of Hungarian PHD and DLA Students (2021) pp. 440, ISBN:9786155586996.

17. **Ghabour, R.**, Korzenszky, P. (2021): Design optimisation and configuration of solar heating system used for pasteurising heat demand in two different regions, *Efficiency, solar and thermal energy for the human comfort*: Book of Abstracts Gödöllő, Hungary: Hungarian University of Agriculture and Life Science (2021) pp. 33-34, ISBN: 9789632699585.
18. Hossain, S., **Ghabour, R.**, Korzenszky, P. (2021): Potential application and system optimization of solar domestic swimming pool heating system in cold climates, *Efficiency, solar and thermal energy for the human comfort*: Book of Abstracts Gödöllő, Hungary: Hungarian University of Agriculture and Life Science (2021) pp. 19-20, ISBN: 9789632699585.
19. **Ghabour, R.**, Korzenszky, P. (2022): Economic and energetic assessment of industrial-scale solar thermal energy in the Visegrád region, *Risk Factors of Food Chain: Book of Abstracts Węgierska Górka, Poland (2022)*, pp. 17, ISBN:9789632698540.

Book chapter in foreign languages:

20. **Ghabour, R.**, Korzenszky, P. (2018): Optimal design of solar-assisted industrial processes considering solar energy hybridized with pasteurizer, *Risk Factors of Food Chain*, 93-96. ISBN:978-963-269-774-1.